

Epitaxial growth of Bi nanowires on Pb-√7 × √3 surface

Siyu Huo(霍思宇), Jieying Li(李洁莹), Yuzhou Liu(刘宇舟), Desheng Cai(蔡德胜), Yitong Gu(谷易通), Haoen Chi(迟浩恩), Wenhui Pang(庞文慧), Gan Yu(于淦), Xiaoying Shi(史晓影), Wenguang Zhu(朱文光), and Shengyong Qin(秦胜勇)

Citation: Chin. Phys. B, 2025, 34 (**10**): 106801. DOI: 10.1088/1674-1056/addeb9
http://cpb.iphy.ac.cn; http://iopscience.iop.org/cpb

What follows is a list of articles you may be interested in

Mode characteristics of nested eccentric waveguides constructed by two cylindrical nanowires coated with graphene

Ji Liu(刘吉), Lixia Yu(于丽霞), and Wenrui Xue(薛文瑞)
Chin. Phys. B, 2022, 31 (**3**): 036803. DOI: 10.1088/1674-1056/ac1e17

Three-dimensional vertical ZnO transistors with suspended top electrodes fabricated by focused ion beam technology

Chi Sun(孙驰), Linyuan Zhao(赵林媛), Tingting Hao(郝婷婷), Renrong Liang(梁仁荣), Haitao Ye(叶海涛), Junjie Li(李俊杰), and Changzhi Gu(顾长志)
Chin. Phys. B, 2022, 31 (**1**): 016801. DOI: 10.1088/1674-1056/ac34fe

Probing thermal properties of vanadium dioxide thin films by time-domain thermoreflectance without metal film

Qing-Jian Lu(陆青鑑), Min Gao(高敏), Chang Lu(路畅), Fei Long(龙飞), Tai-Song Pan(潘泰松), and Yuan Lin(林媛)
Chin. Phys. B, 2021, 30 (**9**): 096801. DOI: 10.1088/1674-1056/abea94

In-plane oriented $CH_3NH_3PbI_3$ nanowire suppression of the interface electron transfer to PCBM

Tao Wang(王涛), Zhao-Hui Yu(于朝辉), Hao Huang(黄昊), Wei-Guang Kong(孔伟光), Wei Dang(党伟), and Xiao-Hui Zhao(赵晓辉)
Chin. Phys. B, 2021, 30 (**6**): 066801. DOI: 10.1088/1674-1056/abf4fa

Temperature-dependent subband mobility characteristics in n-doped silicon junctionless nanowire transistor

Ya-Mei Dou(窦亚梅), Wei-Hua Han(韩伟华), Yang-Yan Guo(郭仰岩), Xiao-Song Zhao(赵晓松), Xiao-Di Zhang(张晓迪), Xin-Yu Wu(吴歆宇), Fu-Hua Yang(杨富华)
Chin. Phys. B, 2019, 28 (**6**): 066804. DOI: 10.1088/1674-1056/28/6/066804

Epitaxial growth of Bi nanowires on Pb-$\sqrt{7} \times \sqrt{3}$ surface

Siyu Huo(霍思宇)[1,2,†], Jieying Li(李洁莹)[1,2,†], Yuzhou Liu(刘宇舟)[1,2], Desheng Cai(蔡德胜)[1,2], Yitong Gu(谷易通)[1,2], Haoen Chi(迟浩恩)[1,2], Wenhui Pang(庞文慧)[1,2], Gan Yu(于淦)[1,2], Xiaoying Shi(史晓影)[1,2], Wenguang Zhu(朱文光)[1,2,3,‡], and Shengyong Qin(秦胜勇)[1,2,3,§]

[1] *International Center for Quantum Design of Functional Materials (ICQD), University of Science and Technology of China, Hefei* 230026, *China*
[2] *CAS (Chinese Academy of Sciences) Key Laboratory of Strongly Coupled Quantum Matter Physics, Department of Physics, University of Science and Technology of China, Hefei* 230026, *China*
[3] *Hefei National Laboratory, University of Science and Technology of China, Hefei* 230088, *China*

(Received 15 April 2025; revised manuscript received 29 May 2025; accepted manuscript online 30 May 2025)

Confining particles in one-dimensional (1D) systems profoundly modifies their electronic behaviors, which have been extensively demonstrated in carbon nanotubes and atomic chains. Structural instabilities and electron localizations often dominate the conductivity of 1D nanowires. Here, we successfully grew Bi single nanowires and nanowire arrays on Pb-$\sqrt{7} \times \sqrt{3}$ substrates via molecular beam epitaxy, both of which exhibit metallic behavior. Using scanning tunneling microscopy and first-principles density functional theory calculations, the interwire coupling and the correlation between nanowire bundles and electronic properties are investigated. A characteristic peak at 0.75 eV is observed on single wires and wire bundles of up to four nanowires, whereas interwire coupling weakens it and makes it disappear for wire bundles of five and above. These findings illustrate that the interwire coupling plays a critical role in the electronic structure of the 1D system, which provides insights for the design of nano-electronics materials.

Keywords: one-dimensional system, nanowire, molecular beam epitaxy, scanning tunneling microscopy, scanning tunneling spectroscopy, interwire coupling, localization

PACS: 68.37.Ef, 71.15.Mb, 73.21.–b, 81.07.–b

DOI: 10.1088/1674-1056/addeb9 **CSTR:** 32038.14.CPB.addeb9

1. Introduction

The exploration of one-dimensional (1D) nanostructures has become a central topic in condensed matter physics in recent decades, particularly in the study of their quantum confinement effect[1,2] and topological properties.[3,4] Among those 1D nanomaterials, nanowires exhibit remarkable potential in fields such as nano-electronics,[5–7] thermoelectrics,[8–10] and optoelectronics.[11–13] At the atomic scale, the interactions between nanowires and their unique topological electronic structures often give rise to new states of matter,[14,15] such as localized 1D edge states at the edges of van der Waals epitaxially grown $ZrTe_5$ arrays and topological edge states at the edges of Bi_4I_4 nanoribbons. Theoretical frameworks such as the Luttinger liquid model[16,17] provide a fundamental description of such 1D systems, although debates on localization mechanisms continue. Abrikosov *et al*. proposed that interwire coupling can suppress localization,[18] while Prigodin *et al*. argued that localization is inevitable even in weakly disordered systems.[19] Recent advancements in the study of sliding Luttinger liquid further reveal how interwire interactions can stabilize exotic quantum phases.[20]

Notably, it has been reported that interwire interactions could dramatically alter the nanowire bundle's electronic structure, for example, in $GdSi_2$ nanowires,[21] where bundles of three or more wires turn metallic while single or double wires stay insulating below 50 K. Similarly, In/Si(111) system achieves metal–insulator transition via the balance of intra- and interwire couplings,[22] and W_6Te_6 nanowires induce semiconductor–metal transitions through van der Waals interwire interactions.[23] Despite these insights into the role of interwire interactions, the precise tuning of the electronic properties of 1D nanostructures through high-quality fabrication remains challenging, highlighting the urgent need for the fabrication of novel 1D nanostructures and exploration of how interwire coupling governs the tuning of their electronic properties.

Bismuth (Bi), has attracted extensive research attention in the field of energy storage,[24,25] thermoelectric materials,[26,27] and topological quantum materials,[28–30] distinguished by its strong spin–orbit coupling (SOC). In particular, the theoretical prediction of nontrivial Z_2 topological properties in ultra-thin Bi(111) films[31] has been confirmed through the observation of higher-order topological insulator states with hinge-localized modes,[32] and its cleaved (111) surface exhibits robust edge states,[33] making it an ex-

[†]These authors contributed equally to this work.
[‡]Corresponding author. E-mail: wgzhu@ustc.edu.cn
[§]Corresponding author. E-mail: syqin@ustc.edu.cn

© 2025 Chinese Physical Society and IOP Publishing Ltd. All rights, including for text and data mining, AI training, and similar technologies, are reserved.

emplary two-dimensional (2D) topological insulator. These characteristics have stimulated extensive research into the epitaxial growth of Bi nanostructures. For example, Bi grown on Si(111)[34] or Ni(111)[35] initially forms a pseudo-cubic Bi(110) bilayer structure, which then evolves into a Bi(111) film influenced by thickness-dependent quantum size effects,[35–37] while on $NbSe_2$ it forms a compressed 2D triangular lattice with 1D ripples.[38,39] Remarkable phenomena include the theoretical predictions of high thermoelectric performance of Bi nanowires[40] and superconductivity below 8.3 K in rhombic Bi nanowires.[41]

In this work, high-quality Bi nanowires were successfully fabricated through precise tuning the molecular beam epitaxy (MBE) process. The fabrication process involves the formation of a Pb-$\sqrt{7}\times\sqrt{3}$ reconstruction[42] on Si(111)-7×7, followed by the deposition of Bi at room temperature, revealing a novel 1D growth mode for Bi monolayers. Through careful adjustment of the epitaxy parameters, we found that Bi nanowires can only be obtained within a narrow flux window. Scanning tunneling spectroscopy (STS) measurements reveal that both individual nanowires and wire bundles exhibit metallic behavior, with nanoscale protrusions distributed on top of the nanowires. Furthermore, we observed a distinctive 0.75 eV peak in the local density of states (LDOS) for bundles with up to four nanowires, which vanishes in wider wire bundles. Density functional theory (DFT) calculations suggest that the disappearance of the characteristic peak is related to interwire coupling. This work highlights the unique electronic signatures of Bi nanowires, providing an effective method for synthesizing 1D Bi nanowires. Furthermore, it offers a promising platform to explore exotic quantum states and 1D superconductivity, with potential applications in nanoelectronics.

2. Methods

The fabrication and characterization of Bi nanowires were performed using home-built integrated MBE-scanning tunneling microscopy (STM)/STS system in an ultra-high vacuum (UHV) chamber with a base pressure of approximately 2.0×10^{-10} Torr (1 Torr = 1.33322×10^{2} Pa). Prior to deposition, n-type Si(111) substrates ($\rho = 0.001$ Ω·cm–0.005 Ω·cm) were degassed at ∼ 600 °C for 6 hours, followed by 14 flashes at 1150 °C in UHV to achieve the clean Si(111)-7×7 reconstructed surface. Pb was first deposited onto this surface at 440 °C for ∼ 5 minutes at room temperature followed by annealing at ∼ 300 °C for 1.5 minutes to form a macroscopically uniform Pb-$\sqrt{7}\times\sqrt{3}$ reconstructed template.[43] Subsequently, Bi was evaporated at a rate of ∼ 0.15 ML/min onto the Pb-$\sqrt{7}\times\sqrt{3}$ surface at room temperature, resulting in the growth of well-ordered, uniform Bi nanowires. The formation of Bi nanowires is highly dependent on the Bi deposition amounts, which can be controlled by adjusting the Bi evaporation time. Different Bi amounts lead to variations in nanowire coverage; however, the morphological characteristics of the nanowires remain unchanged. High-purity Pb (99.999%) and Bi (99.999%) were thermally evaporated from Knudsen cells, and the pressure during MBE growth was maintained below 4.0×10^{-10} Torr to prevent unexpected contamination during the growth process. After the epitaxial growth, samples were immediately transferred to STM equipped with an RHK Pan scanning head and an RHK R9 controller for scanning. Unless otherwise stated, all STM and STS measurements were conducted at ∼ 77 K with a base pressure of 2.0×10^{-10} Torr. STM images were obtained in constant current mode with the bias voltage V applied to the sample, using electrochemically etched tungsten tips. STS spectra were acquired using the standard lock-in method with a bias modulation of 15 mV at 2.23 kHz, and the tunneling spectra were processed using the WSXM program.[44]

3. Results and analysis

Fine tuning of the epitaxy parameters is crucial in the growth of nanowires.[45,46] Here, high quality Bi single nanowires and nanowire bundles consisting of two or more nanowires with atomic spacing were successfully obtained by precise controlling of the Bi coverage. Figure 1(b) shows a representative STM image of the Bi nanowires with typical monolayer atomic height. The formation of Bi nanowires is highly dependent on the Bi coverage. For the Bi coverage less than 1 ML, a large-area PbBi-$3\sqrt{3}\times3\sqrt{3}$ surface reconstruction[47,48] and a small number of nano-islands form, as shown in Fig. 1(a), with the inset showing a zoomed-in $3\sqrt{3}\times3\sqrt{3}$ reconstruction. Nanowire arrays begin to form at Bi coverage of around 1 ML. Figures 1(b) and 1(c) show large-scale STM images of nanowires obtained with Bi coverage of 1.2 ML and 1.5 ML, respectively. Large-area nanowire arrays dominate at 1.2-ML coverage, whereas only sparse short nanowires and abundant 2D nano-islands form at 1.5-ML coverage. A detailed analysis has revealed an interesting observation that the amount of nanowires first increases with Bi coverage, and then decreases for the Bi coverage from 1 ML to 1.5 ML, as shown in Fig. 1(d). As comparisons, we have also tried to deposit an additional 0.3-ML Bi onto pre-formed 1.2-ML Bi nanowires, and identical 2D structures as the previous 1.5 ML in Fig. 1(c) with single continuous deposition were observed, revealing a coverage-dependent evolution regardless of deposition sequences. Furthermore, Bi deposition at liquid nitrogen temperature (77 K) fails to produce nanowires, this might be due to suppressed Bi adatom mobility, highlighting the critical role of thermal activation in nucleation and growth.[49–51]

Figure 1(b) shows that the growth directions of the nanowires typically form 120° angles, matching the trigonal symmetry of the PbBi-$3\sqrt{3}\times 3\sqrt{3}$ structure. Notably, the nanowires are typically limited to the same atomic step terraces during growth. Figure 2(a) displays a zoomed-in STM image of coexisting nanowires and the PbBi-$3\sqrt{3}\times 3\sqrt{3}$ phase. Line profile in Fig. 2(b) (black line marked in Fig. 2(a)) reveals that nanowire has typical 1.27-nm apparent width and 3.9-Å height, the interwire spacing is around 1.80 nm and lengths of nanowires can extend up to tens of nanometers (Fig. 1(b)). The interwire spacing remains consistent across all three growth directions. Please note here that the measured nanowire spacing (1.80 nm) is closed to the experimentally determined period of the triangular $3\sqrt{3}$ phase structure (1.90 nm).

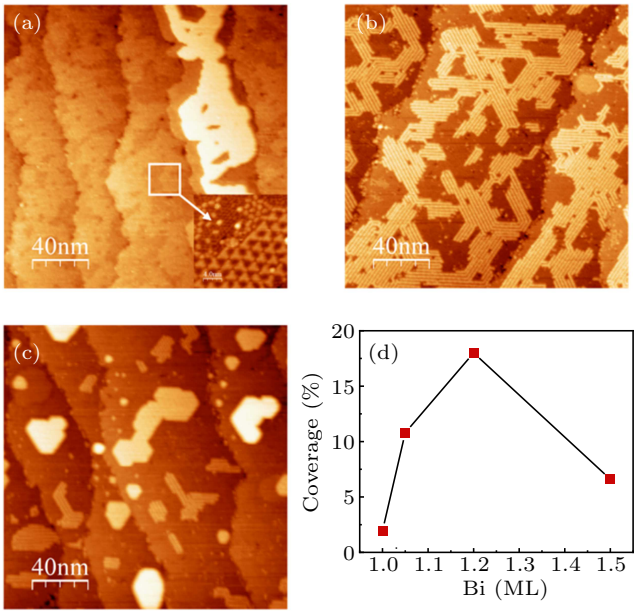


Fig. 1. Epitaxial growth of Bi nanowires on Pb-$\sqrt{7}\times\sqrt{3}$ substrate. (a)–(c) Topographic STM images (200 nm×200 nm, bias voltage $U = +2.0$ V, tunneling current $I_t = 30$ pA) of the morphology of Bi grown on Pb-$\sqrt{7}\times\sqrt{3}$ substrate at room temperature for 0.9-ML, 1.2-ML, and 1.5-ML Bi coverages, respectively, with the inset in (a) showing a zoomed-in image of the PbBi-$3\sqrt{3}\times 3\sqrt{3}$ reconstruction. (d) Coverage of nanowires with different amounts of Bi deposition. The coverage is obtained by averaging the coverage from ten large-area (400 nm×400 nm) STM topographic images.

The successful growth of Bi nanowires with different numbers of constituent wires provides an ideal platform to investigate interwire coupling and their effects on the electronic properties. Here, we performed STS at single nanowire and nanowire bundles, where all measured $\mathrm{d}I/\mathrm{d}V$ spectra display LDOS with finite value at Fermi energy (Fig. 2(c)), revealing a metallic behavior. Interestingly, single wire and nanowire bundles containing up to four wires all exhibit a persistent peak at 0.75 eV, as shown in Fig. 2(c), whereas this characteristic feature vanishes in bundles with five and above nanowires. Notably, the characteristic peak is most prominent in double nanowires, with its intensity gradually diminishing in three- and four-wire bundles. Notably, despite the reported nontrivial Z_2 topological edge states in ultrathin Bi(111) films,[31,33,52] no localized edge states were observed at the ends of the Bi nanowires in our samples.

To better understand the underlying mechanism of the interwire interactions, we performed first-principles DFT calculations by employing the Vienna *Ab initio* Simulation Package (VASP 6.4.0),[53] using a simple chain system as a model (see structural inset in Fig. 2(d)). The Perdew–Burke–Ernzerhof generalized gradient approximation[54] (PBE-GGA) was chosen to describe the accurate exchange–correlation functionals, and the projector-augmented wave method[55,56] was applied to describe valence electrons. The interchain distance was adjusted by modifying the thickness of the vacuum layer along the *b*-axis, ranging from 27 Å to 7 Å. The corresponding gamma-centered Monkhorst–Pack *k*-mesh[57] was sampled as $28\times N\times 1$, where N was increased from 1 to 14. The calculated DOS exhibits that multiple peaks above the Fermi level can be progressively smoothened and suppressed as the interchain distance decreases to 7 Å, as shown in Fig. 2(d), which clearly demonstrates that interchain interactions can effectively modulate the LDOS, highlighting their critical role in tailoring material properties through structural adjustments.

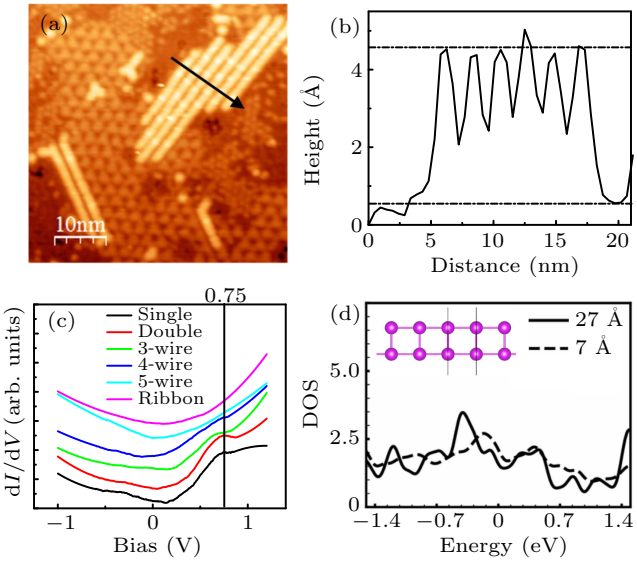


Fig. 2. The STM/S characterization of different wire bundles of Bi nanowires and DFT calculations. (a) Zoomed-in STM image (50 nm×50 nm, $U = +2$ V, $I_t = 50$ pA) of the coexistence region between nanowires and the PbBi-$3\sqrt{3}\times 3\sqrt{3}$ alloy phase. (b) Line profile of the black line in panel (a). (c) Tunneling spectra at nanowires containing single wire and wire bundles, with "ribbon" referring to bundles formed by more than five wires, there is a shift along the vertical axis between different wires. (d) Calculated evolution of DOS with interchain distance decreasing from 27 Å (isolated single chain) to 7 Å (multi-chain bundle). Inset: top-view of structural model of simple simulated chain system for Bi nanowires from DFT calculations.

First-principles DFT calculations further elucidate that isolated nanowires enhance 1D quantum confinement and generate an LDOS peak at 0.75 eV. As the bundle size increases, strengthened interwire coupling promotes electronic delocalization through enhanced interchain transitions, progressively homogenizing the LDOS and suppressing the characteristic

peak.[58,59] While this work advances the understanding of this mechanism, further experimental and computational investigations will focus on elucidating the intricate atomic structures and associated topological properties in future work.

Another interesting observation of the Bi nanowires is the existence of distinct bright protrusions on the top of the nanowires (see Fig. 3(a)). The line profiles measured along the nanowires (the blue line profile in Fig. 3(a)) indicate that these protrusions have an average height of 0.76 Å above the nanowires (see Fig. 3(b)). The statistical analysis of 40 randomly sampled protrusions across different nanowires (see Fig. 3(c)) demonstrates that, accounting for measurement uncertainties, over 92% exhibit inter-protrusion spacing differences of 3.08 Å. This value closely aligns with the intralayer atomic spacing of Bi(00l) (3.07 Å),[60] which may give us some hint about the crystallographic orientation of the Bi nanowires.

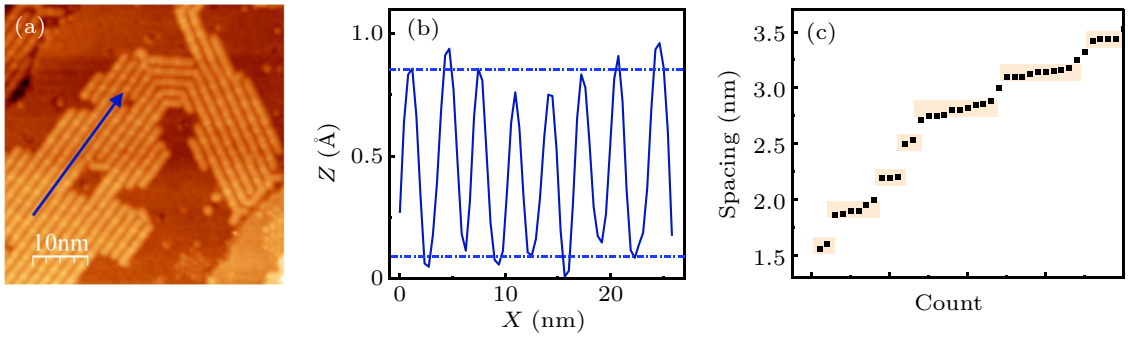


Fig. 3. The STM characterization and statistical analysis of protrusions on Bi nanowires. (a) Zoomed-in topographic images (50 nm×50 nm, $U = +2.0$ V, $I_t = 40$ pA) revealing distinct protrusions on top of the Bi nanowires. (b) Line profile of the blue line in panel (a). (c) Statistical distributions of the spacings between neighboring bright protrusions.

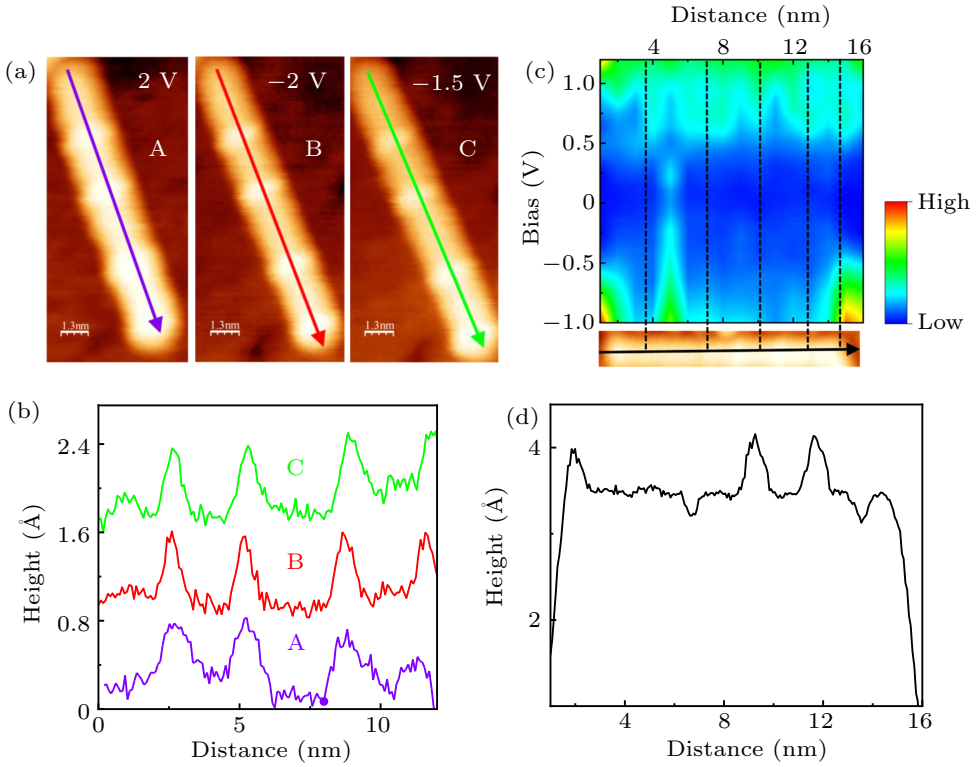


Fig. 4. The STM/S characterization of the nanowire structure: (a) zoomed-in STM images of a single Bi nanowire at three different sample biases of +2 V, −2 V, and −1.5 V, respectively ($I_t = 40$ pA); (b) line profiles along the nanowire at three different sample biases. Profile curves C and B are shifted by 0.8 Å for clarity relative to B and A, respectively. (c) The spatial variations of $\mathrm{d}I/\mathrm{d}V$ spectra as a function of energy along a wire. Black dashed lines mark the locations of terraces with higher electronic density of states compared to protrusions. (d) Line profile of the black line in panel (c).

To rule out the possibility that these protrusions are manifestations of the electronic states, we take the topographic images across a wide bias range (−2 V to 2 V). Figure 4(a) presents STM images of a single nanowire acquired at different biases, all exhibiting the same bright protrusions. Height profiles along the nanowire (Fig. 4(b)) reveal in-phase filled and empty states for both nanowires and protrusions, confirming that these features originate from the actual atomic structure rather than electronic density variations. This behavior closely resembles the results observed in $GdSi_2$ nanowires.[21]

To better understand the electronic structures of the nanowires, we measured the spatial distribution of the STS along the nanowires. Figure 4(c) reveals a higher LDOS at the 0.75-eV characteristic peak on wires than on protrusions, as highlighted by the vertical dashed lines and figure 4(d) presents the line profile of the nanowire. The observed LDOS variation might tentatively correlate with structural differences. Notably, in double nanowires, protrusion-induced chain segmentation could intensify 1D localization,[61] amplifying the characteristic peak.

4. Conclusion

In summary, through precise tuning of epitaxial parameters, we successfully synthesized Bi nanowires as 1D metallic conductors. The coverage of the nanowires can be modulated by adjusting the Bi deposition amount. Despite structural protrusions, all nanowires (isolated wires and wire bundles) maintain metallic behavior. STS reveals a distinct 0.75-eV peak in both isolated wires and small bundles (up to four nanowires), which diminishes in larger assemblies. DFT simulations demonstrate that reduced interchain spacing (27 Å to 7 Å) suppresses localized states above the Fermi level, mirroring experimental observations. Our analysis attributes the peak to be stabilized by the electronic localization in isolated nanowires. Increasing wire bundle size strengthens interwire coupling, which leads to electronic delocalization and spectral homogenization. This work establishes a controllable pathway for 1D Bi nanostructure synthesis, serving as ideal platforms for further exploring the underlying mechanism of interwire coupling and provides critical insights for designing nanowire devices.

Acknowledgements

Project supported by the National Natural Science Foundation of China (Grant Nos. 12374196, 92165201, and 11634011), the Innovation Program for Quantum Science and Technology (Grant No. 2021ZD0302800), the CAS Project for Young Scientists in Basic Research (Grant No. YSBR-046), the Fundamental Research Funds for the Central Universities (Grant Nos. WK3510000006 and WK3430000003), and the Initiative Project in Quantum Information Technologies of Anhui Province, China (Grant No. AHY170000).

References

[1] Yan K, Zhang L, Kuang Q, Wei Z, Yi Y, Wang J and Yang S 2014 *ACS Nano* **8** 3771
[2] Tian Y, Sakr M R, Kinder J M, Liang D, MacDonald M J, Qiu R L, Gao H J and Gao X P 2012 *Nano Lett.* **12** 6492
[3] Hong S S, Zhang Y, Cha J J, Qi X L and Cui Y 2014 *Nano Lett.* **14** 2815
[4] Liu P, Williams J R and Cha J J 2019 *Nat. Rev. Mater.* **4** 479
[5] Cao L, Ang Y S, Wu Q and Ang L K 2020 *Phys. Rev. B* **101** 035422
[6] Rogers J A 2010 *Nat. Nanotechnol.* **5** 698
[7] Wu D J, Jiang S M and Liu X J 2012 *Chin. Phys. B* **21** 077803
[8] Boukai A I, Bunimovich Y, Tahir K J, Yu J K, Goddard I W A and Heath J R 2008 *Nature* **451** 168
[9] Goktas N I, Wilson P, Ghukasyan A, Wagner D, McNamee S and LaPierre R 2018 *Appl. Phys. Rev.* **5** 041305
[10] Zhang Z and Chen J 2018 *Chin. Phys. B* **27** 035101
[11] Sutter P, French J S, Khorashad L K, Argyropoulos C and Sutter E 2021 *Nano Lett.* **21** 4335
[12] Park I, Jin K H, Kim K W and Kim J 2025 *Small* **21** 2409249
[13] Wang D Q, Zhou Z Y, Zhu R and Ye X Y 2008 *Chin. Phys. B* **17** 3875
[14] Xu Y J, Cao G H, Li Q Y, Xue C L, Zhao W M, Wang Q W, Dou L G, Du X, Meng Y X, Wang Y K, Gao Y H, Jia Z Y, Li W, Ji L L, Li F S, Zhang Z Y, Cui P, Xing D Y and Li S C 2024 *Nat. Commun.* **15** 4784
[15] Zhuang J, Li J, Liu Y, Mu D, Yang M, Liu Y, Zhou W, Hao W, Zhong J and Du Y 2021 *ACS Nano* **15** 14850
[16] Luttinger J M 1963 *J. Math. Phys.* **4** 1154
[17] Barak G, Steinberg H, Pfeiffer L N, West K W, Glazman L, Von O F and Yacoby A 2010 *Nat. Phys.* **6** 489
[18] Abrikosov A A and Ryzhkin I A 1978 *Adv. Phys.* **27** 147
[19] Prigodin V N 1997 *Synth. Met.* **84** 705
[20] Begum S, Fleurov V, Kagalovsky V and Yurkevich I V 2019 *J. Phys.: Condens. Matter* **31** 425601
[21] Qin S, Kim T H, Zhang Y, Ouyang W, Weitering H H, Shih C K, Baddorf A P, Wu R and Li A P 2012 *Nano Lett.* **12** 938
[22] Ahn J, Byun J, Koh H, Rotenberg E, Kevan S and Yeom H 2004 *Phys. Rev. Lett.* **93** 106401
[23] Deng J, Huo D, Bai Y, Guo Y, Pan Z, Lu S, Cui P, Zhang Z and Zhang C 2020 *Nano Lett.* **20** 8866
[24] Ni J, Bi X, Jiang Y, Li L and Lu J 2017 *Nano Energy* **34** 356
[25] Wang A, Hong W, Li L, Guo R, Xiang Y, Ye Y, Zou G, Hou H and Ji X 2022 *Energy Storage Mater.* **44** 145
[26] Witting I T, Chasapis T C, Ricci F, Peters M, Heinz N A, Hautier G and Snyder G J 2019 *Adv. Electron. Mater.* **5** 1800904
[27] He S, Bahrami A, Zhang X, Martínez I G, Lehmann S and Nielsch K 2022 *Adv. Mater. Technol.* **7** 2100953
[28] Hirahara T, Fukui N, Shirasawa T, Yamada M, Aitani M, Miyazaki H, Matsunami M, Kimura S, Takahashi T, Hasegawa S and Kobayashi K 2013 *Phys. Rev. Lett.* **110** 149901
[29] Sabater C, Gosalbez M D, Fernandez R J, Rodrigo J G, Untiedt C and Palacios J J 2013 *Phys. Rev. Lett.* **110** 176802
[30] Drozdov I K, Alexandradinata A, Jeon S, Nadj P S, Ji H, Cava R J, Bernevig B A and Yazdani A 2014 *Nat. Phys.* **10** 664
[31] Liu Z, Liu C X, Wu Y S, Duan W H, Liu F and Wu J 2011 *Phys. Rev. Lett.* **107** 136805
[32] Schindler F, Wang Z, Vergniory M G, Cook A M, Murani A, Sengupta S, Kasumov A Y, Deblock R, Jeon S, Drozdov I, Bouchiat H, Gueron S, Yazdani A, Bernevig B A and Neupert T 2018 *Nat. Phys.* **14** 1067
[33] Wada M, Murakami S, Freimuth F and Bihlmayer G 2011 *Phys. Rev. B* **83** 121310
[34] Nagao T, Sadowski J T, Saito M, Yaginuma S, Fujikawa Y, Kogure T, Ohno T, Hasegawa Y, Hasegawa S and Sakurai T 2004 *Phys. Rev. Lett.* **93** 105501
[35] Bollmann T R J, Van G R, Zandvliet H J W and Poelsema B 2012 *Phys. Rev. Lett.* **109** 176102
[36] Kowalczyk P J, Mahapatra O, Le Ster M, Brown S A, Bian G, Wang X and Chiang T C 2017 *Phys. Rev. B* **96** 205434
[37] Gao Q and Widom M 2013 *Phys. Rev. B* **88** 144102
[38] Fang A, Adamo C, Jia S, Cava R J, Wu S C, Felser C and Kapitulnik A 2018 *Sci. Adv.* **4** 0330
[39] Fuseya Y, Katsuno H, Behnia K and Kapitulnik A 2021 *Nat. Phys.* **17** 1031
[40] Lu P X, Zhang M, Zou W J and Kong C 2017 *J. Mater. Res.* **32** 2405
[41] Tian M, Wang J, Kumar N, Han T, Kobayashi Y, Liu Y, Mallouk T E and Chan M H W 2006 *Nano Lett.* **6** 2773

[42] Brochard S, Artacho E, Custance O, Brihuega I, Baró A M, Soler J M and Gómez-Rodríguez J M 2002 *Phys. Rev. B* **66** 205403
[43] Brun C, Cren T, Cherkez V, Debontridder F, Pons S, Fokin D, Tringides M C, Bozhko S, Ioffe L B, Altshuler B L and Roditchev D 2014 *Nat. Phys.* **10** 444
[44] Horcas I, Fernandez R, Gomez-Rodriguez J M, Colchero J, Gomez H J and Baro A M 2007 *Rev. Sci. Instrum.* **78** 013705
[45] Krogstrup P, Ziino N, Chang W, Albrecht S, Madsen M, Johnson E, Nygård J, Marcus C M and Jespersen T 2015 *Nat. Mater.* **14** 400
[46] Zhao S, Fathololoumi S, Bevan K, Liu D, Kibria M, Li Q, Wang G, Guo H and Mi Z 2012 *Nano Lett.* **12** 2877
[47] Li P, Xie K, Li L, Li X, Xia Y, Zhang R and Qin S 2022 *Phys. Status Solidi B* **259** 2200095
[48] Li P, Xie K, Xia Y, Cai D and Qin S 2023 *Chin. Phys. B* **32** 066101
[49] He L, Cheng G, Zhu Y and Park H S 2023 *Nano Lett.* **23** 5779
[50] McCreary K, Pi K, Swartz A, Han W, Bao W, Lau C, Guinea F, Katsnelson M and Kawakami R 2010 *Phys. Rev. B* **81** 115453
[51] Patel S B, Li C, Al-Mahboob A, Sadowski J T and Zhou G 2025 *J. Am. Chem. Soc.* **147** 1656
[52] Gao C L, Qian D, Liu C H, Jia J F and Liu F 2013 *Chin. Phys. B* **22** 067304
[53] Kresse G and Furthmuller J 1996 *Phys. Rev. B* **54** 11169
[54] Perdew J P, Burke K and Ernzerhof M 1996 *Phys. Rev. Lett.* **77** 3865
[55] Kresse G and Joubert D 1999 *Phys. Rev. B* **59** 1758
[56] Blöchl P E, Först C J and Schimpl J 2003 *Bull. Mater. Sci* **26** 33
[57] Methfessel M and Paxton A T 1989 *Phys. Rev. B* **40** 3616
[58] Chandrasekaran N, Gann E, Jain N, Kumar A, Gopinathan S, Sadhanala A, Friend R H, Kumar A, McNeill C R and Kabra D 2016 *ACS Appl. Mater.* **8** 20243
[59] Martens H 2006 *Phys. Rev. Lett.* **96** 076603
[60] Dong C, Liu Y and Qi Y 2018 *Acta Metall. Sin.* **54** 935
[61] Fogler M M, Teber S and Shklovskii B 2004 *Phys. Rev. B* **69** 035413